Control of chemical release in hydrogel microvalve array for localized chemical stimulations

Nafis Mustakim[1], Youngsik Song[1], A.H. Rezwanuddin Ahmed[2] and Sang-Woo Seo[1*]

[1]Department of Electrical Engineering, The City College of New York,

[2]Department of Biomedical Engineering, The City College of New York

160 Convent Avenue,

New York, NY 10031, USA

*Corresponding Author

Email: swseo@ccny.cuny.edu

Abstract

Chemical stimulation is considered one of the most promising therapeutic solutions for degenerated retina due to its ability to mimic a natural chemical signaling pathway. However, the majority of demonstrated platforms actuate chemicals using bulky external setups. Hence, developing high-resolution chemical release platforms with remote-controlled actuation mechanism is of great interest to the next generation of chemical prosthetics. Moreover, the effectiveness of chemical stimulation depends on several parameters, such as the chemical dosage, pulse duration, and spread radius. Therefore, to engineer the chemical release profile, the actuation mechanism of these localized chemical release platforms needs to be thoroughly studied to facilitate modifications. In this study, we have presented a high-resolution chemical release platform based on a macroporous silicon membrane structure. Chemical release ports defined in the membrane pores can be remotely actuated through thermo-responsive poly(N-isopropylacrylamide) (PNIPAAm) hydrogel with near-infrared (NIR) light. As plasmonic heating elements, gold nanorod (GNR) was incorporated within PNIPAAm hydrogel. The pore size of the hydrogel was tuned by varying tetrahydrofuran content in the hydrogel polymerization solution. We have shown that the chemical release properties through membrane pores can be controlled as required using this approach. This insight can be used to engineer the relevant chemical release parameters, thereby creating an efficient chemical stimulation platform.

Keywords:

Thermo-responsive hydrogel, PNIPAAm hydrogel, Microfluidic valve,
Localized chemical release, light-actuated valve

1. Introduction

Signal transduction between neurons is carried out by chemical substances known as neurotransmitters [1]. However, the degeneration of neurons damages this signal propagation from one neuron to another, resulting in the loss of their functional activities. Existing therapeutic solutions for treating degenerated neurons include oral drugs, neurosurgery, and prosthetic stimulation [2]. Among them, for retinal degeneration, prosthetic electrical stimulation is the most clinically proven solution to regain visual perception [3], [4]. Although electrical stimulation has made tremendous advancements in recent times, it is far from reaching the level of biological spatial resolution and specificity [5]. Moreover, excessive heat generation from a large number of electrodes can damage the retina cells. [6], [7], [8], [9]. It also fails to mimic the specificity offered by biological systems that can address individual cell types [10]. In recent times, chemical stimulation has garnered attention for addressing the limitations of electrical stimulation as it mimics the retinal synapse by releasing neurotransmitters to stimulate the retinal cells [11], [12].

An artificial synaptic platform for stimulating retinal synapses should have neurotransmitter release sites with spatial resolution ideally reaching individual cells. Whenever signal transduction takes place, each site should be capable of continuously regulating specific amounts of neurotransmitters on its own, considering that synapses in the retina release neurotransmitters continuously, and their release rates are modulated in response to the graded membrane potential variation [13]. Researchers have already demonstrated the efficacy of localized chemical stimulation of retina cells with artificial prosthetic devices [14], [15], [16]. Most of these works still involve the use of external tubing or injection systems to control the release of neurotransmitters. However, for practical applications, chemical actuation needs to be remotely controlled in the implanted retinal prosthetic. Some efforts to incorporate advanced actuation mechanisms into the release ports have been demonstrated with electroosmosis and ionic polarization diode [17], [18]. But no multiport release platform with remotely controlled actuation capability has been demonstrated.

Stimuli-responsive polymers have opened a new door for the reliable, controlled release of chemicals in biological systems [19]. Leveraging the benefits of stimuli-responsive polymer, a unique device with high-density fluidic ports has been proposed for localized chemical release applications [20]. The port of the devices is composed of the thermo-responsive PNIPAAm hydrogel-graphene column, which can release chemicals upon NIR illumination. They utilized the release of chemicals due to hydrogel contraction and fluid flow from the gap created between

hydrogel and channel wall due to hydrogel shrinking. However, the effect of PNIPAAm composition on chemical release behavior is yet to be studied. This is particularly important because the amount of chemical released, the chemical spread radius, and the pulse parameters play a crucial role in the chemical stimulation of retina cells [24]. Control of the release parameters by tuning the composition of the hydrogel will open a new way for engineering released chemical parameters to increase the efficacy of chemical stimulation of the neuron cells of the retina.

In this paper, we have proposed high-density, three-dimensional microfluidic ports containing light-actuated microvalves whose release property can be readily tuned. The arrayed microvalve is composed of temperature-sensitive PNIPAAm hydrogel which is covalently attached to the pore walls of a macroporous silicon (MPS) membrane. The microvalve can be actuated remotely with NIR light through gold nanorod (GNR) embedded in the hydrogel polymer network. As the hydrogel is covalently bonded to the walls, chemical transportation is possible only through the interconnected porous path of the hydrogel microvalve. NIR illumination modulates the path in the arrayed microvalve, resulting in the chemical release characteristics. By tuning the hydrogel pore size with tetrahydrofuran (THF), we have been able to control the amount of chemicals released through the microvalve. As the pore size of the PNIPAAm network increases, more rapid chemical actuation is observed. This work will help to engineer the PNIPAAm microvalve to meet the desired release parameters needed for a highly efficient localized chemical release platform.

2. Design and Fabrication

2.1 Design of the arrayed microvalve

Fig. 1 illustrates the schematic of the proposed device studied in this work. The device utilizes a high-density pore configuration in a MPS membrane. The top side of the membrane works as a two-dimensional array of stimulation sites. Each site can be remotely activated by a hydrogel microvalve covalently attached to the side wall of the pore. The PNIPAAm microvalves contained in the pores of the MPS membrane can be viewed as a porous polymer block with interconnected flow paths. When the temperature in the hydrogel goes beyond the Lower critical solution temperature (LCST), The polymer-polymer interaction dominates, and the whole polymer network collapses. Since the microvalve is rigidly bonded with the side wall of the substrate with surface primer reagent, the polymer network will be stretched towards the side walls. As a result, the pores inside the PNIPAAM matrix, which act as fluidic

channels, will be enlarged. Therefore, the resistance towards fluidic flow will decrease subsequently. The microvalve is considered “open” in this state. But when the temperature of the polymer network is below the LCST, the polymer network becomes swollen. The swollen polymer matrix causes the pore to shrink thus seizing the liquid flow through the pore. Therefore, the microvalve goes to the “closed” state.

The pore size of the PNIPAAm matrix was increased through the addition of THF in the hydrogel polymerization process. It has been demonstrated that when THF is added during the polymerization of PNIPAAm, it acts as a foaming and precipitating agent [25]. Therefore, the resulting hydrogel is more porous than the conventional form. The pore size can also be increased by increasing the ratio of THF volume to polymerization solution volume [26]. To demonstrate the impact of hydrogel pore size on chemical release through the MPS membrane, we prepared three different compositions of PNIPAAm by varying THF content in the polymerization solution.

2.2 Materials

N-isopropyl acrylamide (NIPAAm), 3-(trimethoxysilyl)propyl methacrylate (TMSPMA), Silver Nitrate ($AgNO_3$), and Tetrahydrofuran (THF) were purchased from TGI America. N,N’-Methylene-bis- acrylamide (BIS), ascorbic acid ($C_6H_8O_6$) Polyvinylpyrrolidone (PVP), 4,4'-Azobis(4-cyanopentanoic acid) (ACVA) and Perfluorodecyltrichlorosilane (FDTS) were purchased from VWR. Fluorescein sodium salt, Chloroauric acid ($HAuCl_4$), Sodium borohydride ($NaBH_4$), and Hexadecyltrimethylammonium bromide (CTAB) were purchased from Sigma Aldrich. All chemicals were used as received.

2.3 Preparation of arrayed PNIPAAm microvalve

Fig. 3 illustrates the process flow diagram of the arrayed microvalve device. First, the one-side opened MPS sample was purchased from Smart Membrane, Germany, and the pore was opened following the same protocol previously mentioned in [20]. The pores are ~400 µm long with a diameter of ~ 9µm and a pitch distance of ~ 12µm. Fig.2 (a) shows a scanning electron microscope and Fig.2 (b), (c) show the optical microscope images of the front and back sides of the MPS, respectively. The sample is treated with oxygen plasma for 5 min at 100W and (flow rate: 20 sccm). Then, the sample was soaked in 2 vol% TMSPMA Solution for 30 min. The TMSPMA solution is prepared by adding 1 mL of TMSPMA in 50 mL of Deionized (DI) water containing 5 µL of Acetic Acid. The sample was sonicated for 5s to remove unbound TMSPMA from the surface, followed by thorough rinsing with DI water. Next,

the sample was baked in the furnace at 70°C. The hydrogel precursor solution was prepared by mixing 1.112 g NIPAAm, 55.6 mg BIS, 22.21 mg of ACVA, and 1mL of THF (for 10 vol% THF in water) in 10 mL of water. For preparing hydrogel compositions with 2.5 vol% and 5 vol% THF in water, the amount of THF was varied accordingly, keeping similar chemical compositions. The hydrogel precursor solutions were mixed with PVP-coated GNR and degassed for 1 hr before UV exposure. The GNR is synthesized following the seed-mediated method discussed previously in [22].

Degassed hydrogel precursor solution with GNR was added to a cubic silicone mold containing the TMSPMA-treated membrane sample. An FDTS-treated glass substrate was then placed on the membrane sample as a weight. The silicone mold was then transferred to a desiccator, and pressure was reduced to ~ -1 Bar. As a result, the polymerization solution could fill up the pores of the MPS sample. Then, the sample was placed in an ice bath and cured with 365nm UV light using Hypercure-200, Hologenix for 7 min. After the UV Curing, the sample was kept in clean DI water and the FDTS-treated glass substrate could easily be detached from the membrane sample with a tweezer. Excess hydrogel attached to the sample from the sides was removed with a razor blade. All the samples were fabricated following the same procedure.

3. Result and discussion

3.1 Characterization of photothermal conversion

Fig. 4(a) shows the normalized Vis-IR transmission of the GNR measured with an AQ-4303B white light source and a Filmmetrics spectrometer. Spectral dips around 500 nm and 800 nm in the optical transmission spectra of the synthesized GNR. Due to the localized surface plasmon resonance (LSPR), absorption is dominant in these wavelengths. The most dominant absorption is around the NIR region at 800 nm. Since the NIR light can penetrate deeper into the biological tissue and incur low absorption loss, the microvalve can be remotely controlled when implanted for in vivo application [27].

A bulk hydrogel sample was placed on a glass slide and irradiated with collimated laser beam at λ=815 nm in continuous wave mode. The corresponding temperature was measured with an FLIR i7 (FLIR system, USA) camera with a 5s interval. Fig. 4(b) shows the temperature increase of the PNIPAAm hydrogel samples with time when irradiated with 350 mW laser power. The temperature increases rapidly in the beginning but saturates over time. Moreover, the temperature response of hydrogel samples is also observed as shown in Fig. 4(c). Hydrogel precursor solutions containing 2.5 vol%, 5 vol%, and 10 vol% THF in polymerization solution were mixed with equal amounts of GNR. In all the cases, the temperature starts to increase rapidly from room temperature and gradually saturates after 40s. The rates of the temperature increase in the hydrogel with different pore sizes show a negligible variation. Since only GNR contributes to the temperature, pore size variation is not expected to bring any significant difference in the time-temperature response of the PNIPAAm hydrogel.

3. 2 Thermo-responsive operation of arrayed microvalve

The optical light transmission through the arrayed microvalve sample was analyzed to confirm successful PNIPAAm confinement inside the pores. The sample was placed in an aluminum block and the intensity of the light transmitted through the sample was recorded with a digital microscope camera. The backside of the aluminum block had a window to allow light to pass through the sample as shown in Fig.5 (a). The block was filled with water and placed under a microscope, and the temperature of it was controlled with a digital temperature controller. Fig. 5(b) and (c) show the image of the sample before and after the PNIPAAm microvalve. Since PNIPAAm is optically

transparent at room temperature, light can still pass through the pores of the sample. However, the intensity of the transmitted light through the membrane has decreased compared to a sample without PNIPAAm microvalve. When the temperature is increased to 40℃, which is higher than the typical LCST temperature of PNIPAAm, the integrated microvalve turns completely opaque blocking the light completely. As a result, only a dark window can be seen in Fig. 5(d).

Fig. 6 illustrates the change of intensity of the transmitted light through the arrayed microvalves as a function of temperature. The same experimental setup, as shown in Fig. 5(a), was used to record this measurement. With a digital temperature controller, the temperature was increased from 25℃ to 42℃. Data was recorded 5 min after reaching the set point temperature so that the PNIPAAm had enough time to respond to the change. It can be seen in Fig. 6 that the intensity of light transmitted through the sample is almost constant from 26℃ to 34℃. Since this temperature range is lower than LCST, the microvalve remains in the "closed" state in this temperature range. As the temperature reaches the LCST of the hydrogel, the intensity of the light transmission drops sharply at 34℃. This is because hydrogel starts to become opaque at a temperature higher than LCST temperature. The hydrogel in this state starts to shrink and the pore size increases. In this case, the microvalve transitions from the "closed" to the "open" state. But no more significant variation in the intensity of the transmitted light is observed at ~ 37℃. This implies that the microvalves have gone through complete phase transformation, and the pores inside the PNIPAAm matrix attain maximum size. Beyond this temperature, the microvalve will remain completely in the "open" state. Fig. 6 also shows that the thermal response of the arrayed microvalves with different THF contents does not show any significant variation. Since THF content determines the pore sizes inside the hydrogel matrix, the thermo-responsive optical property of the PNIPAAm might not be affected significantly. By copolymerizing its monomer with different distinct monomers, the phase transition temperature required to stimulate the PNIPAAm hydrogel action can be adjusted to closely match the physiological temperature of cells [21]. It can also be actuated within 4℃ of its temperature variation [20], [22]. As seen in Figure 6, our proposed microvalve actually requires about 2℃ to fully open. The required heat to regulate our valve operation can be safe for stimulating neurons as it has been reported that neuron cells can be damaged when the temperature is increased to 60℃ with a pulsed infrared laser [23].

3.3 NIR light-actuated operation of arrayed microvalve

The sample is placed in the aluminum block mentioned in section 3.2 under a custom-modified microscope, as shown in Fig. 7(a). An 815 nm laser source was used to remotely actuate the valve operation. The red circle in Fig. 7(a) represents the sample region illuminated with the NIR light. Fig. 8(a) and 8(b) show the sample with and without NIR light illumination, respectively. The region of the sample where the laser is illuminated turns dark as the temperature in that region increases beyond LCST, and the corresponding PNIPAAm microvalves of that region become oblique.

The normalized intensity of light through the sample can be observed in Fig. 7(b) when irradiated with the laser pulse of 5s ON-5s OFF time. During the ON cycle, the temperature in the irradiated area goes beyond LCST. As a result, the intensity of the light through the arrayed microvalve starts to decrease, indicating the valve begins to open. Again, during the OFF state, the arrayed microvalves become transparent, indicating the valve is closed. Intensity decreases comparatively slowly in the ON cycle as it takes some time to build up temperature. However, the temperature quickly dissipates to the surrounding water during the OFF cycle. Moreover, when the laser power is increased from 110 mW to 150 mW, light intensity is reduced more rapidly. However, when laser power is increased to 190 mW, no significant difference in the intensity compared to 150 mw response can be seen. Once the temperature of the arrayed microvalve rises beyond ~ 37℃, the intensity change through the arrayed microvalves saturates, as observed in Fig.6. This indicates that when the sample is illuminated with 110 mW optical power, the microvalve is not partially opened. But when illuminated with 150 mW and 190 mW laser power, the valve inside the pore can be completely opened.

Fig. 8(a) shows the schematic of the experimental setup used for monitoring localized chemical release through the MPS membrane. Fluorescein dye has been used as a model chemical to understand the chemical release property of the arrayed microvalve. To prevent dye accumulation in the laser-irradiated area, the front side of the membrane is constantly flushed with DI water at a flow speed of 77 μL/min. The reservoir consists of a 0.2M Fluorescent solution prepared by dissolving fluorescein sodium salt in DI water. As shown in Fig. 8 (d), when the NIR is off, no variation in the dye intensity can be observed. But when the NIR is illuminated, the valve opens, and consequently, dye is released. As a result, the fluorescent intensity increases in that local area, as shown in Fig. 8 (e).

The dynamic dye response when the microvalve is actuated by 5s ON-7s OFF laser pulse can be observed in supplementary video 1.

The dynamic dye release through the arrayed microvalve is illustrated in Fig. 9 where the pulse of 5s ON-5s OFF time is applied. During ON cycles, the dye intensity increases as the microvalves open in the illuminated area. During the OFF cycle, the dye intensity decreases as the valve is closed. When laser power increases to 150 mW from 110 mW, more rapid dye intensity change is observed, suggesting an increase in the amount of released dye through the valve. As stated in section 3.2, the microvalve is partially opened with 110 mW and fully opened with 150 mW. Thus, the amount of chemical release can be controlled with laser power. But once the valve is completely opened the amount of released chemical cannot be further increased by increasing the laser power. Due to this reason, the dye release behavior with 150 mW and 190 mW pulses do not show significant variation.

3.4 Effect of pore size variation on chemical release behavior

Fig. 10 illustrates the variation in dye release through the microvalve as the pore size in the PNIPAAm matrix is enlarged. As mentioned, the pore size in the hydrogel matrix has been tuned by varying the THF content in the hydrogel composition. The higher the THF content, the larger the pore size of the PNIPAAm matrix. Fig. 9 (a) and (b) illustrate that the change in normalized intensity of the dye is more rapid when illuminated with NIR light as THF content is increased during the polymerization of the PNIPAAm matrix. This result implies that the amount of dye flowing through the porous PNIPAAm matrix is a function of the pore size inside the matrix. Because of the enlarged pore, a higher amount of dye can pass through the opened microvalve compared to the one with a smaller pore size. So, the modulation amplitude of the dye intensity is highest for the arrayed microvalve having 10 vol% THF concentration in the polymerization solution. As the THF content is decreased in the polymerization solution, the modulation amplitude of fluorescent intensity decreases.

However, during the OFF cycle, it takes more time for the actuated region's fluorescent intensity to go back to the initial condition if the THF content is higher. This is because diffusion through pores in the PNIPAAm hydrogel matrix might be higher when the valve is OFF (or naturally closed). To evaluate the diffusion through the microvalve, we have observed the natural dye diffusion through the arrayed microvalve. The same experimental setup and condition as stated in Fig.8 (a) is used, but the laser was kept off during this experiment. The flushing water was also

turned off to capture the diffused dye amount through the closed microvalve. The change in the normalized dye intensity was recorded using the microscope camera. The natural diffusion of the dye through the arrayed microvalve in the closed state is illustrated in Fig. 11. Moreover, to observe how dye would diffuse if no microvalve is present, diffusion through a porous silicon sample without any PNIPAAm microvalve is also shown in Fig. 11. When no microvalve is present, dye is diffused rapidly, and the diffusion saturates within 15s. For samples with microvalve, the dye diffusion rate is much smaller than the sample with no microvalve. The dye, in small quantities, can pass through the pores of the hydrogel matrix when the microvalve is in the OFF (naturally closed) state. The presence of THF regulates the pore size of the hydrogel matrix during polymerization. The diffusion of dye is highest through the hydrogel microvalve composed of 10% THF because of its largest pore size and lowest through the hydrogel matrix pore formed by 2.5% THF. This property of the PNIPAAm microvalve can help regulate the neurotransmitter release rate as a chemical prosthetic for the retina. Since the release behavior affects the efficacy of the chemical stimulation, having control over the release property of the microvalve could be a powerful tool to achieve optimum stimulation of neuron cells.

4. Conclusion

We demonstrate the effect of the PNIPAAm microvalve property on the chemical release behavior of remotely controlled multi-site chemical prosthetics. The proposed platform is a MPS membrane with a pore diameter of 9μm, channel length of 400μm, and pitch length of 12 μm. Each pore acts as a stimulation site, and the release of neurotransmitters from the pore can be remotely controlled by NIR light. To control the chemical flow, each pore has an integrated PNIPAAm hydrogel that acts as a valve. GNR is incorporated inside the PNIPAAm microvalve to control the flow with NIR light remotely. The valve is covalently bonded with the inner side wall of the porous silicon membrane. So, the flow of chemical-contained liquid is possible only through the microvalve. The microvalve has a porous network that remains expanded when the NIR light is off i.e., the valve is OFF. When the NIR light is ON, the PNIPAAm network collapses and liquid can flow freely. The pore size can be increased by increasing the THF content in PNIPAAm precursor during the polymerization. The increased pore size results in a more rapid release of chemicals during actuation. Such control on liquid release behavior can pave the way for designing PNIPAAm arrayed microvalve having the most efficient release behavior of neurotransmitter during localized chemical stimulation.

Acknowledgment

This work was supported by CUNY PSC-CUNY grant and National Science Foundation grant (NSF-1952469).

Author Contribution

N. Mustakim and S. Seo conceived the idea and designed the research. N. Mustakim and A.H.R. Ahmed performed the experiments. N. Mustakim, Y. Song, and S. Seo analyzed the results. N. Mustakim drafted the manuscript and all authors contributed to the writing of the manuscript.

Declarations

Conflict of Interests The authors declare no competing interests.

Reference

[1] S. E. Hyman, "Neurotransmitters.," *Curr Biol*, vol. 15, no. 5, pp. R154–R158, Mar. 2005, doi: 10.1016/j.cub.2005.02.037.

[2] A. Jonsson *et al.*, "Bioelectronic neural pixel: Chemical stimulation and electrical sensing at the same site," *Proc Natl Acad Sci U S A*, vol. 113, no. 34, pp. 9440–9445, Aug. 2016, doi: 10.1073/PNAS.1604231113/SUPPL_FILE/PNAS.201604231SI.PDF.

[3] M. S. Humayun, E. de Juan, and G. Dagnelie, "The Bionic Eye: A Quarter Century of Retinal Prosthesis Research and Development," *Ophthalmology*, vol. 123, no. 10, pp. S89–S97, Oct. 2016, doi: 10.1016/J.OPHTHA.2016.06.044.

[4] E. Zrenner *et al.*, "Subretinal electronic chips allow blind patients to read letters and combine them to words," *Proceedings of the Royal Society B: Biological Sciences*, vol. 278, no. 1711, pp. 1489–1497, 2011, doi: 10.1098/RSPB.2010.1747.

[5] S. Inayat, C. M. Rountree, J. B. Troy, and L. Saggere, "Chemical stimulation of rat retinal neurons: feasibility of an epiretinal neurotransmitter-based prosthesis," *J Neural Eng*, vol. 12, no. 1, p. 016010, Dec. 2014, doi: 10.1088/1741-2560/12/1/016010.

[6] C. M. Rountree, A. Raghunathan, J. B. Troy, and L. Saggere, "Prototype chemical synapse chip for spatially patterned neurotransmitter stimulation of the retina ex vivo," *Microsystems & Nanoengineering 2017 3:1*, vol. 3, no. 1, pp. 1–12, Nov. 2017, doi: 10.1038/micronano.2017.52.

[7] M. C. Peterman *et al.*, "Localized Neurotransmitter Release for Use in a Prototype Retinal Interface," *Invest Ophthalmol Vis Sci*, vol. 44, no. 7, pp. 3144–3149, Jul. 2003, doi: 10.1167/IOVS.02-1097.

[8] E. Zrenner, "Fighting Blindness with Microelectronics," *Sci Transl Med*, vol. 5, no. 210, Nov. 2013, doi: 10.1126/SCITRANSLMED.3007399.

[9] C. D. Eiber, N. H. Lovell, and G. J. Suaning, "Attaining higher resolution visual prosthetics: a review of the factors and limitations*," *J Neural Eng*, vol. 10, no. 1, p. 011002, Jan. 2013, doi: 10.1088/1741-2560/10/1/011002.

[10] S. Inayat, C. M. Rountree, J. B. Troy, and L. Saggere, "Chemical stimulation of rat retinal neurons: feasibility of an epiretinal neurotransmitter-based prosthesis," *J Neural Eng*, vol. 12, no. 1, p. 016010, Dec. 2014, doi: 10.1088/1741-2560/12/1/016010.

[11] P. G. Finlayson and R. Iezzi, "Glutamate Stimulation of Retinal Ganglion Cells in Normal and S334ter-4 Rat Retinas: A Candidate for a Neurotransmitter-Based Retinal Prosthesis," *Invest Ophthalmol Vis Sci*, vol. 51, no. 7, pp. 3619–3628, Jul. 2010, doi: 10.1167/IOVS.09-4877.

[12] K. Sou, D. L. Le, and H. Sato, “Nanocapsules for Programmed Neurotransmitter Release: Toward Artificial Extracellular Synaptic Vesicles,” *Small*, vol. 15, no. 17, p. 1900132, Apr. 2019, doi: 10.1002/SMLL.201900132.

[13] C. W. Morgans, “Neurotransmitter release at ribbon synapses in the retina,” *Immunol Cell Biol*, vol. 78, no. 4, pp. 442–446, Aug. 2000, doi: 10.1046/J.1440-1711.2000.00923.X.

[14] C. M. Rountree, J. B. Troy, and L. Saggere, “Microfluidics-Based Subretinal Chemical Neuromodulation of Photoreceptor Degenerated Retinas,” *Invest Ophthalmol Vis Sci*, vol. 59, no. 1, pp. 418–430, Jan. 2018, doi: 10.1167/IOVS.17-23142.

[15] M. C. Peterman *et al.*, “Localized Neurotransmitter Release for Use in a Prototype Retinal Interface,” *Invest Ophthalmol Vis Sci*, vol. 44, no. 7, pp. 3144–3149, Jul. 2003, doi: 10.1167/IOVS.02-1097.

[16] M. C. Peterman *et al.*, “The Artificial Synapse Chip: A Flexible Retinal Interface Based on Directed Retinal Cell Growth and Neurotransmitter Stimulation,” *Artif Organs*, vol. 27, no. 11, pp. 975–985, Nov. 2003, doi: 10.1046/J.1525-1594.2003.07307.X.

[17] Y. Hu *et al.*, “Neuromodulation using electroosmosis,” *J Neural Eng*, vol. 18, no. 4, p. 046072, Jun. 2021, doi: 10.1088/1741-2552/AC00D3.

[18] T. A. Sjöström, A. Jonsson, E. O. Gabrielsson, M. Berggren, D. T. Simon, and K. Tybrandt, “Miniaturized Ionic Polarization Diodes for Neurotransmitter Release at Synaptic Speeds,” *Adv Mater Technol*, vol. 5, no. 3, p. 1900750, Mar. 2020, doi: 10.1002/ADMT.201900750.

[19] A. Zhang, K. Jung, A. Li, J. Liu, and C. Boyer, “Recent advances in stimuli-responsive polymer systems for remotely controlled drug release,” *Prog Polym Sci*, vol. 99, p. 101164, Dec. 2019, doi: 10.1016/J.PROGPOLYMSCI.2019.101164.

[20] H. Rostami Azmand, Y. Song, and S. W. Seo, “Light–controlled hydrogel platform for high-resolution chemical stimulation,” *Sens Actuators A Phys*, vol. 346, p. 113809, Oct. 2022, doi: 10.1016/J.SNA.2022.113809.

[21] M. J. Ansari *et al.*, “Poly(N-isopropylacrylamide)-Based Hydrogels for Biomedical Applications: A Review of the State-of-the-Art,” *Gels 2022, Vol. 8, Page 454*, vol. 8, no. 7, p. 454, Jul. 2022, doi: 10.3390/GELS8070454.

[22] Y. Song, H. Rostami Azmand, and S. W. Seo, “Rapid photothermal actuation of light-addressable, arrayed hydrogel columns in a macroporous silicon membrane,” *Sens Actuators A Phys*, vol. 301, p. 111729, Jan. 2020, doi: 10.1016/J.SNA.2019.111729.

[23] W. G. A. Brown *et al.*, “Thermal damage threshold of neurons during infrared stimulation,” *Biomed Opt Express*, vol. 11, no. 4, p. 2224, Apr. 2020, doi: 10.1364/BOE.383165.

[24] C. M. Rountree, J. B. Troy, and L. Saggere, “Investigation of Injection Depth for Subretinal Delivery of Exogenous Glutamate to Restore Vision via Biomimetic Chemical Neuromodulation,” *IEEE Trans Biomed Eng*, vol. 67, no. 2, pp. 464–470, Feb. 2020, doi: 10.1109/TBME.2019.2915255.

[25] X. Z. Zhang and C. C. Chu, “Preparation of thermosensitive PNIPAAm hydrogels with superfast response,” *Chemical Communications*, vol. 0, no. 3, pp. 350–351, Jan. 2004, doi: 10.1039/B313073H.

[26] G. Chen, F. Svec, and D. R. Knapp, “Light-actuated high pressure-resisting microvalve for on-chip flow control based on thermo-responsive nanostructured polymer,” *Lab Chip*, vol. 8, no. 7, pp. 1198–1204, Jun. 2008, doi: 10.1039/B803293A.

[27] Y. Qian, S. Lu, J. Meng, W. Chen, and J. Li, “Thermo-Responsive Hydrogels Coupled with Photothermal Agents for Biomedical Applications,” *Macromol Biosci*, p. 2300214, 2023, doi: 10.1002/MABI.202300214.

Figure Captions

Figure 1. Schematic of the arrayed PNIPAAM microvalve proposed in this study.

Figure 2. (a) Scanning Electron Microscope image of the sample taken at 45° angle (100 μm scale bar). Optical microscope image of the (b) frontside and (c) backside of the sample. The scale bar is 50 μm for (b) and (c).

Figure 3. Schematic fabrication processes of arrayed PNIPAAm microvalve.

Figure 4. (a) Normalized Vis-IR transmission spectra of as-synthesized gold nanorod. (b) Time-temperature response of a bulk PNIPAAm sample when irradiated with an 815 nm laser source. (C) Time-temperature response of PNIPAAm hydrogel compositions with varying pore sizes irradiated with a 350 mW/cm^2 collimated laser beam.

Figure 5. (a) Schematic of the experimental setup to observe the light transmitted through the membrane sample. (b) Optical image of the membrane sample without PNIPAAm microvalve (c) Optical image of the membrane sample with arrayed microvalve at room temperature. (d) Optical image of the membrane sample with arrayed microvalve at 40°C.

Figure 6. Normalized light transmission through the membrane pore with different THF contents in PNIPAAm microvalves.

Figure 7. (a) Schematic of the experimental setup for photothermal actuation of transmitted light through the membrane sample. (b) The normalized light intensity as a function of time when actuated with varying laser power of 5s ON cycle and 5s OFF cycle.

Figure 8(a) Schematic of the experimental setup for observing dye transport through arrayed microvalve. Optical microscope image of light transmitted through the membrane when the laser is in (b) OFF cycle and (c) ON cycle (taken with experimental setup of 7(a)). Optical microscope image of the membrane under UV illumination when the laser is in (d) OFF cycle and (e) ON cycle.

Figure 9 Normalized dye intensity of the fluorescent dye released through the arrayed microvalve with varying laser power when irradiated with laser pulse of 5s ON time and 5s OFF time.

Figure 10 Normalized intensity of the fluorescent dye released through the arrayed microvalve when porosity in hydrogel matrix is varied with the addition of THF. The microvalve is actuated with the laser pulse of (a) 5s ON-5s OFF cycle at 110 mW and (b) 5s ON-7s OFF cycle at 150 mW.

Figure 11 Natural diffusion of dye through the PNIPAAm microvalve as a function of time.

Figure 1

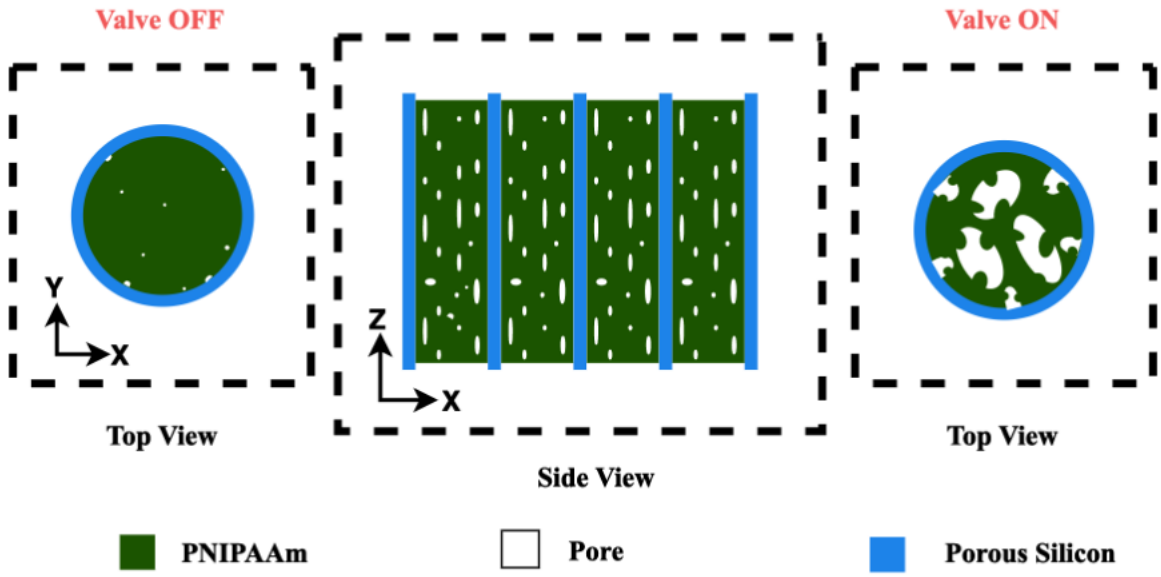
Valve OFF
Valve ON
Y
X
Z
X
Top View
Side View
Top View
PNIPAAm
Pore
Porous Silicon

Figure 2

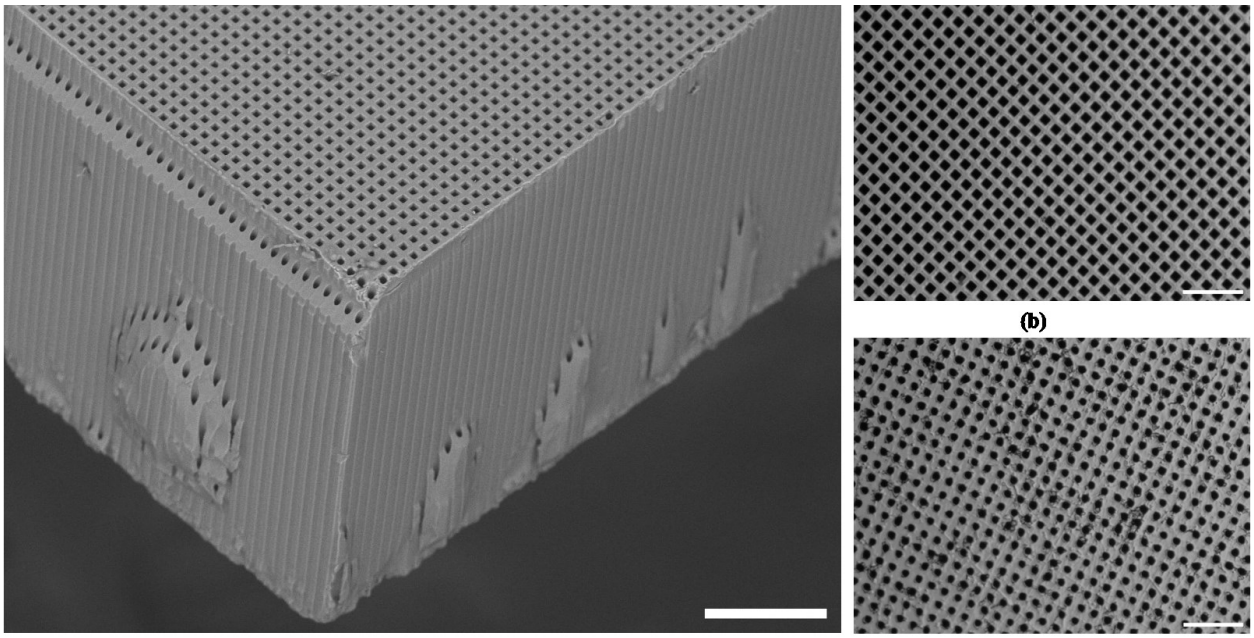

(a)

(b)

(c)

Figure 3

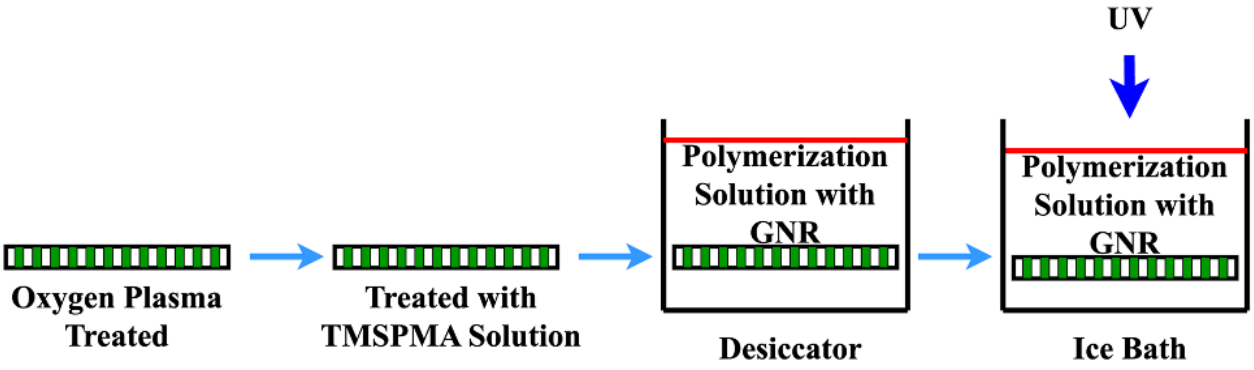
UV
Polymerization Solution with GNR
Polymerization Solution with GNR
Oxygen Plasma Treated
Treated with TMSPMA Solution
Desiccator
Ice Bath

Figure 4

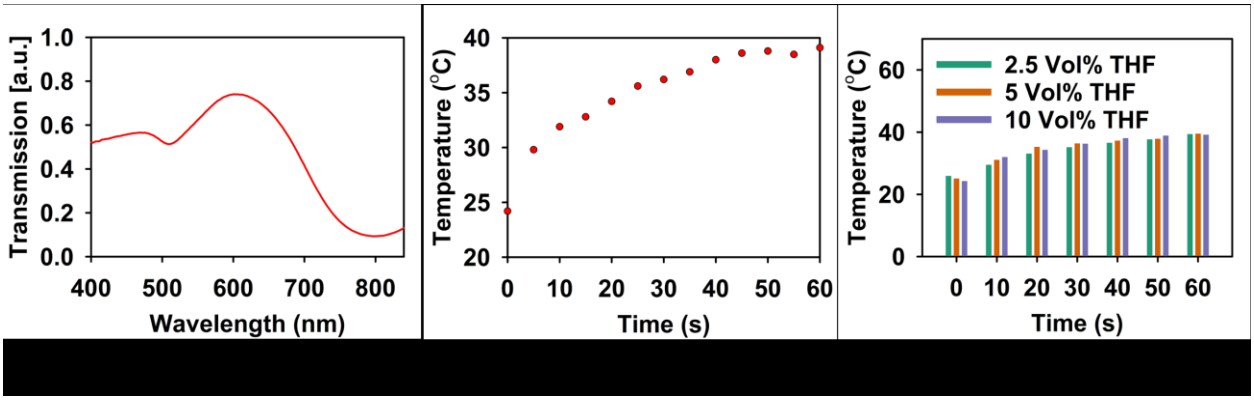
Transmission [a.u.]
1.0
0.8
0.6
0.4
0.2
0.0
400
500
600
700
800
Wavelength (nm)
Temperature (°C)
40
35
30
25
20
0
10
20
30
40
50
60
Time (s)
Temperature (°C)
60
40
20
0
2.5 Vol% THF
5 Vol% THF
10 Vol% THF
0
10
20
30
40
50
60
Time (s)

Figure 5

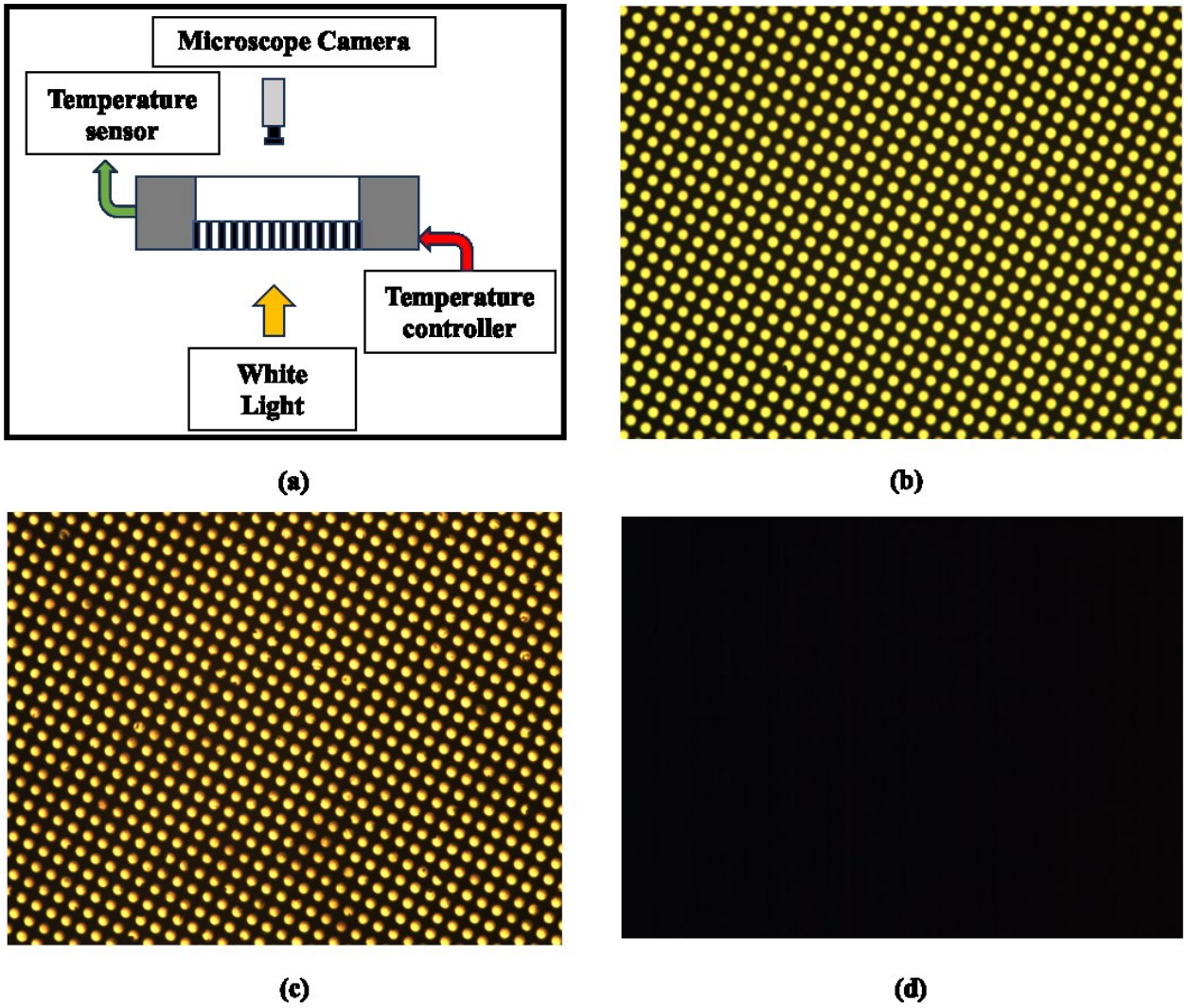
Microscope Camera
Temperature sensor
Temperature controller
White Light
(a)
(b)
(c)
(d)

Figure 6

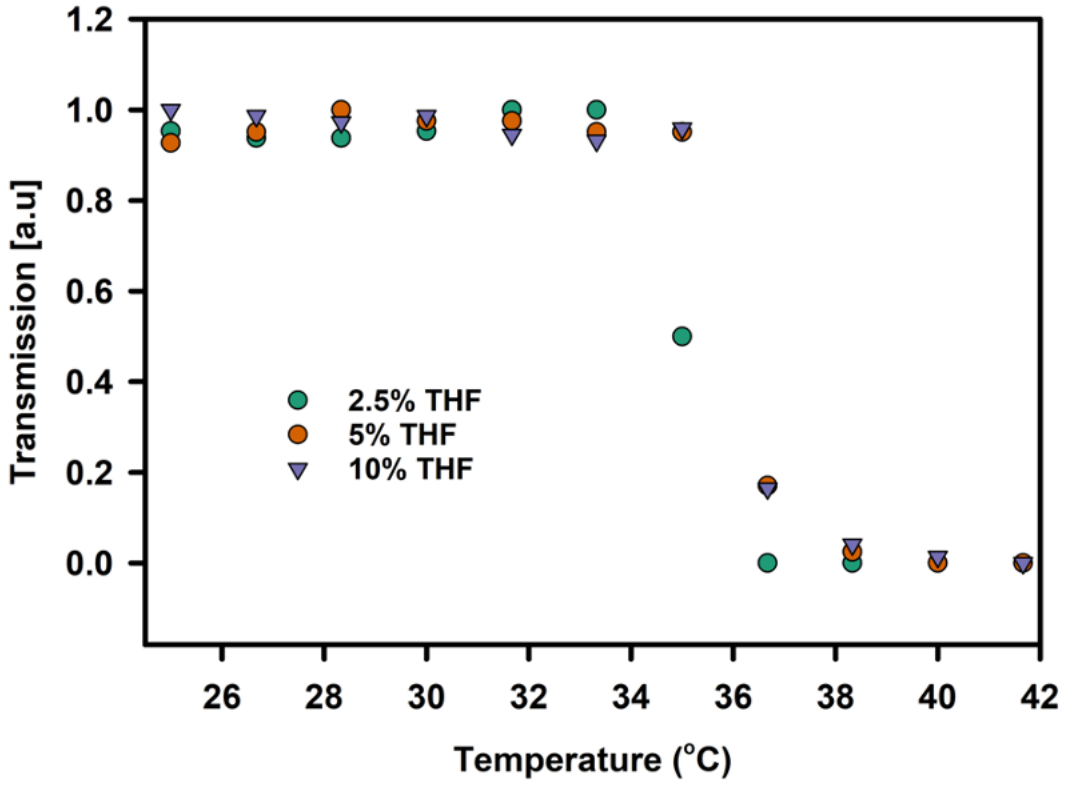
1.2
1.0
0.8
0.6
0.4
0.2
0.0
Transmission [a.u]
2.5% THF
5% THF
10% THF
26
28
30
32
34
36
38
40
42
Temperature (°C)

Figure 7

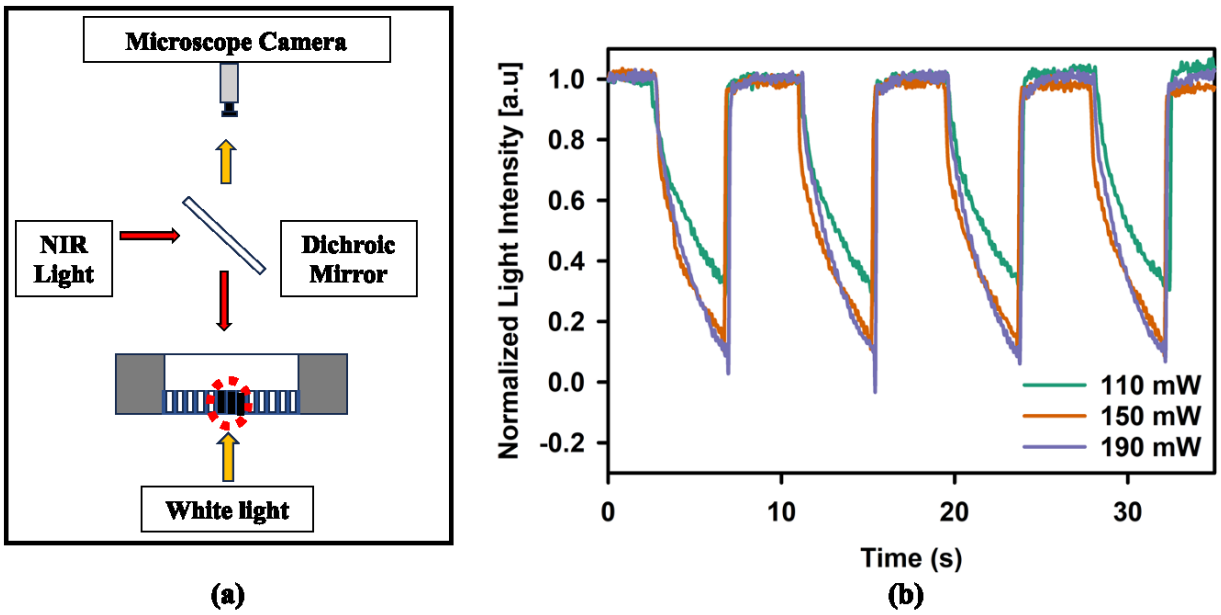
Microscope Camera
NIR Light
Dichroic Mirror
White light
(a)
Normalized Light Intensity [a.u]
1.0
0.8
0.6
0.4
0.2
0.0
-0.2
0
10
20
30
Time (s)
110 mW
150 mW
190 mW
(b)

Figure 8

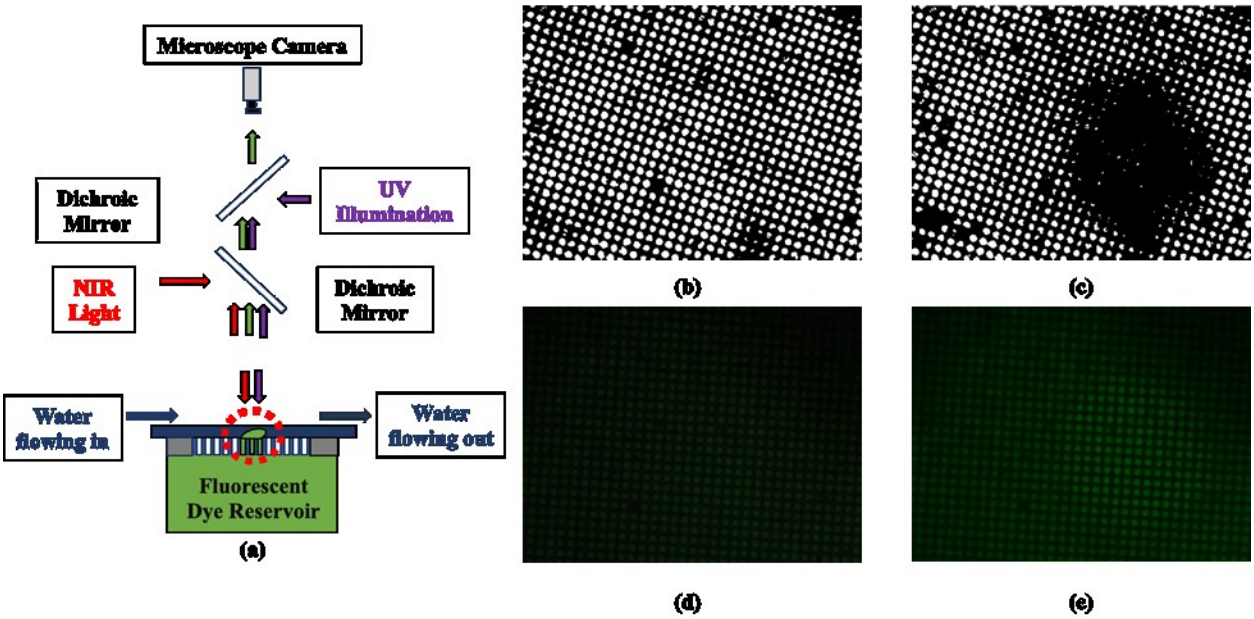
Microscope Camera
Dichroic Mirror
UV Illumination
NIR Light
Dichroic Mirror
Water flowing in
Water flowing out
Fluorescent Dye Reservoir
(a)
(b)
(c)
(d)
(e)

Figure 9

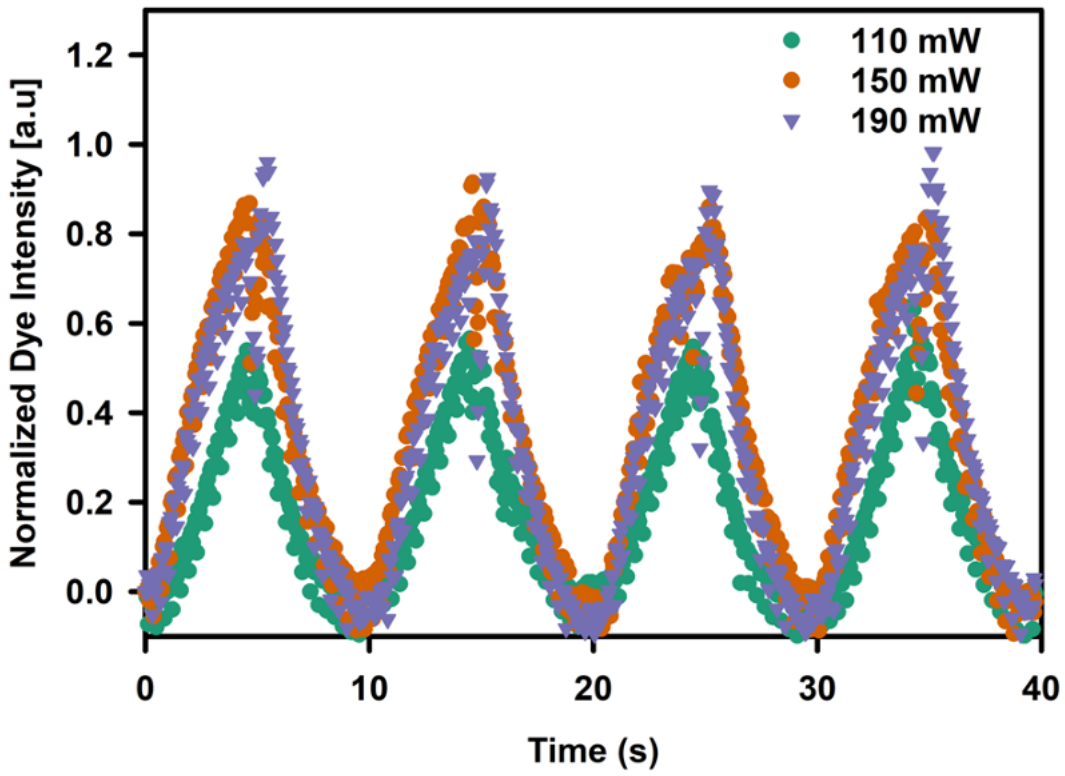
110 mW
150 mW
190 mW
Normalized Dye Intensity [a.u]
1.2
1.0
0.8
0.6
0.4
0.2
0.0
0
10
20
30
40
Time (s)

Figure 10

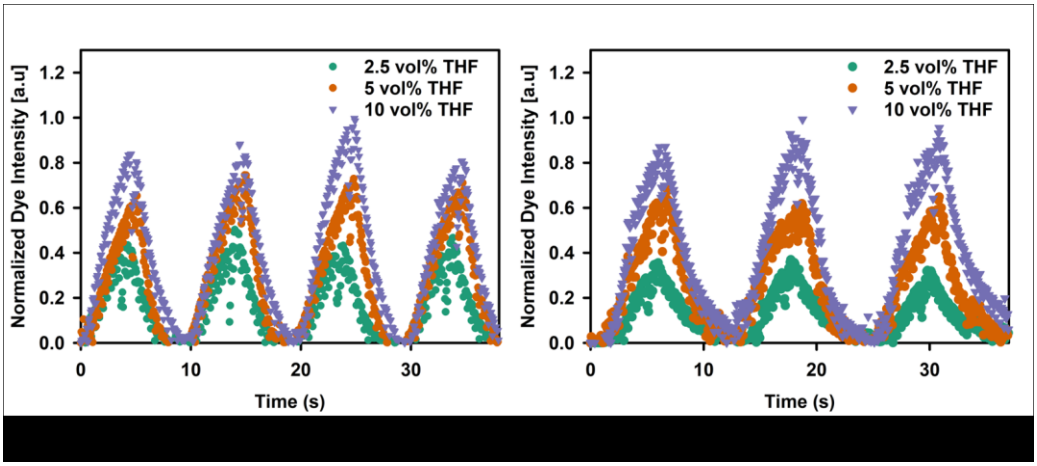
Normalized Dye Intensity [a.u]
1.2
1.0
0.8
0.6
0.4
0.2
0.0
0
10
20
30
Time (s)
2.5 vol% THF
5 vol% THF
10 vol% THF
Normalized Dye Intensity [a.u]
1.2
1.0
0.8
0.6
0.4
0.2
0.0
0
10
20
30
Time (s)
2.5 vol% THF
5 vol% THF
10 vol% THF

Figure 11

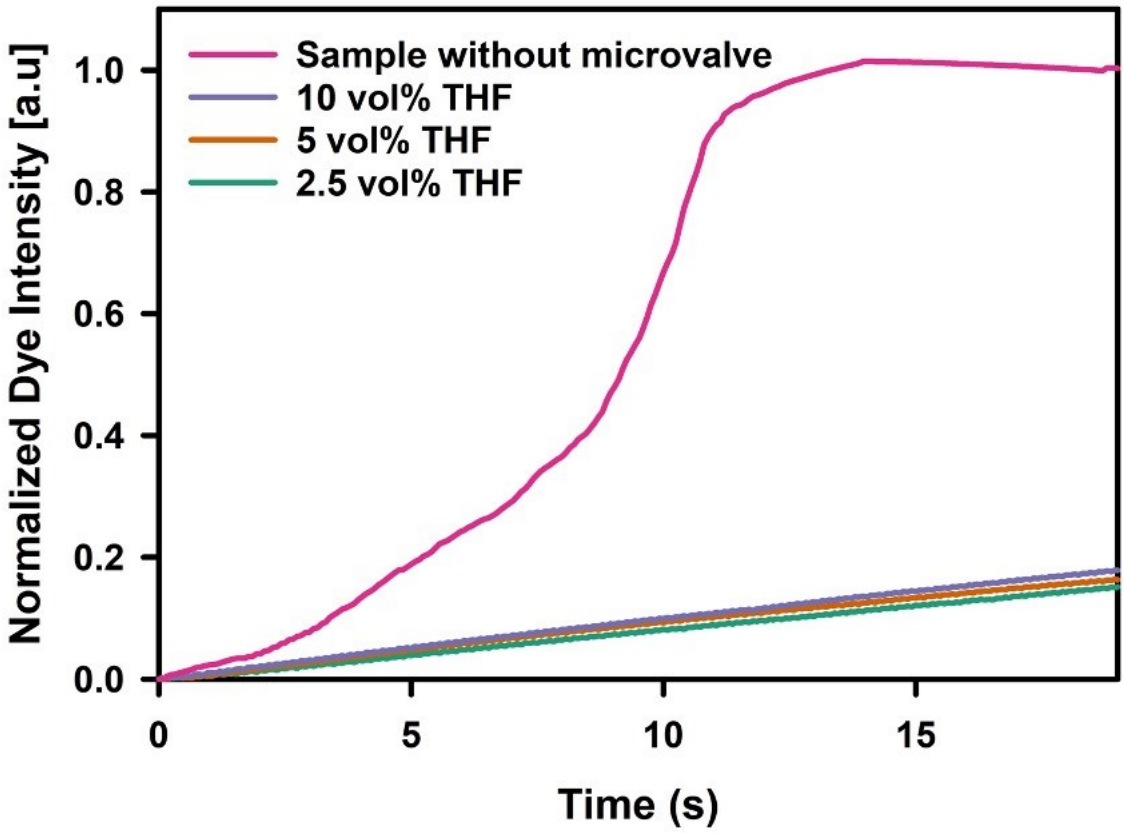
Sample without microvalve
10 vol% THF
5 vol% THF
2.5 vol% THF
Normalized Dye Intensity [a.u]
1.0
0.8
0.6
0.4
0.2
0.0
0
5
10
15
Time (s)

Supplementary Video:

Video 1. Dynamic dye response of the membrane sample with PNIPAAm microvalve when irradiated with 110 mW NIR pulse of 5s ON-7s OFF cycle.